Article:
Papatheou, E., Manson, G., Barthorpe, R.J. et al. (2014) The use of pseudo-faults for damage location in SHM: An experimental investigation on a Piper Tomahawk aircraft wing. Journal of Sound and Vibration, 333 (3). pp. 971-990. ISSN: 0022-460X

https://doi.org/10.1016/j.jsv.2013.10.013

The Use of Pseudo-Faults for Damage Location in SHM: An Experimental Investigation on a Piper Tomahawk Aircraft Wing

Evangelos Papatheou, Graeme Manson, Robert J. Barthorpe, Keith Worden

Dynamics Research Group, Department of Mechanical Engineering, University of Sheffield, Mappin Street, Sheffield S1 3JD, UK

Abstract

The application of pattern recognition-based approaches in damage localisation and quantification will eventually require the use of some kind of supervised learning algorithm. The use, and most importantly, the success of such algorithms will depend critically on the availability of data from all possible damage states for training. It is perhaps well known that the availability of damage data through destructive means cannot generally be afforded in the case of high value engineering structures outside laboratory conditions. This paper presents the attempt to use added masses in order to identify features suitable for training supervised learning algorithms and then subsequently test the trained classifiers with damage data, with the ultimate purpose of damage localisation. In order to test the approach of adding masses, two separate cases of a dual-class classification problem, representing two distinct locations, and a three-class problem representing three distinct locations, are examined with the help of a full-scale aircraft wing. It was found that an excellent rate of correct classification could be achieved in both the dual-class and three-class cases. However, it was also found that the rate of correct classification was sensitive to the choices made in training the supervised learning algorithm. The results for the dual-class problem demonstrated a comparatively high level of robustness to these choices with a substantially lower robustness found in the three-class case.

Keywords:
added mass, vibration-based, damage localisation

1. Introduction

The earliest possible detection of damage in structures is vital for their safety and also for the avoidance of the high costs which could be conveyed if it is left to develop. The traditional non-destructive evaluation (NDE) methods [1] are currently the main inspection tool. Although they are highly effective, they have certain disadvantages regarding their use, which include among others, general limitations to accessible areas of the structure, high demand on expertise and also their high inspection costs. In addition, NDE methods work in a local vicinity and so usually they necessitate the *a priori* knowledge of the area of interest. Structural health monitoring (SHM) has emerged as a potential answer to the drawbacks of the NDE techniques. The possibility of an on-line monitoring tool which could reduce the cost of lengthy NDE inspections has made the field of SHM a highly active research area. Comprehensive reviews on SHM are [2, 3].

Inside the general framework of damage identification, the effort to locate damage has always been inherent, and an extensive review of those efforts is out of the scope of this work, references

can again be found in [2, 3]. In general, many approaches are validated against numerical and/or experimental laboratory structures of the beam or plate type, and recent examples are [4–6]. The approaches followed include variants of mode shape curvature/modal strain energy e.g. [7] and model updating inverse problems [8] among others. Supervised learning algorithms such as Artificial Neural Networks (ANN) have also been extensively used as in [9, 10].

In the last ten years, damage detection has been widely accepted as a problem of pattern recognition (PR) [11], and not only as a model-driven inverse problem. Any approach to locate or assess damage (in addition to the identification of its presence) with PR approaches will probably make use of some kind of supervised learning algorithm. The use of such algorithms will inevitably demand data from all damage states of interest to be used as examples. It is possible to acquire such data when dealing with inexpensive small-scale structures in a laboratory environment, but it will become a serious obstacle when testing damage detection methods on high-value structures, such as aircraft. In any such case, destructive means of introducing faults will not be an affordable solution.

To alleviate the previously mentioned problem, without the use of high-fidelity models, the authors have attempted to test a very simple idea. In the effort to extract features capable of indicating damage without actually damaging the structure, the blithe extrapolation of a SDOF formula for the natural frequency ($\omega = \sqrt{k/m}$), allows for the assumption that perhaps the addition of a mass would be enough to generate training data for supervised learning algorithms. This idea is not revolutionary since several attempts to test damage detection algorithms with mass addition have been made before as in [12–14]. In addition, specifically added mass localisation was done in [15] with the help of a concentrated mass on a rectangular plate, while in [16] added masses were additionally assessed in terms of their weight in an attempt to perform damage severity on an aircraft skeleton wing.

However, despite the previous use of added mass as a proxy for damage, the effort to test the suitability of a mass as a pseudo-fault and use it to train algorithms, then subsequently test with 'realistic' damage has been attempted in [17] involving only preliminary results and more thoroughly in [18]. In both those cases the problem was addressed only as level one detection in Rytter's scale [19] (i.e. the detection of the presence of the fault only). The purpose of this paper is to present the attempt to use added mass data to train supervised learning algorithms in order to *locate* 'real' damage. Two separate cases are examined, a dual-class and a three-class classification problem. The choice of the problems was based on the logical and progressive extrapolation of the added mass approach which started from [18]. In addition, a dual-class classification problem can be easily approached in an unsupervised approach where a three-class problem cannot generally be solved in such a way.

The layout of the paper is as follows. The next section describes the test procedure and the data acquisition for both the dual and the three-class problems. The second section explains the general feature selection procedure and the localisation of the added masses. The third section describes the performance of the added mass trained locator on damage data for the two-class problem while the fourth section discusses the three-class location problem. Finally, the paper is rounded off with some overall conclusions and a discussion of the future potential of the approach.

2. Test procedure

The main purpose of this paper is to develop a damage locator based on added masses and then benchmark it on data originating from damage introduced in the form of saw-cuts. While

it is acknowledged that the introduction of a sawcut is in itself an imperfect proxy for damage it is nevertheless sufficiently representative of an open crack to allow the effectiveness of the approach to be explored, and the sawcut data is referred to herein as the 'real' damaged state data. Since previous attempts [18] have shown that the best features (i.e. parts of data which are able to distinguish between damage states) created from the use of pseudo-faults perform equally well on the case of 'real' damage (the same applies to the worst features in the sense that they perform equally badly), it would be reasonable to think that such an attempt might be successful. The important point here is that the overall attempt to build the locator is 'tuned' using the added masses *only* and with no interaction from data coming from saw-cuts.

The methodology which was used for the location problem is based on previous work in which damage location in a Gnat aircraft wing on the basis of changes in transmissibility spectra was investigated [20]. The structure of interest in the present study was a Piper Tomahawk aircraft wing featuring a number of removal inspection panels. Copies of these inspection panels with a diagonal saw-cut were produced so that they could replace intact panels and provide a valid fault. This tactic was judged best for the currently presented work since the structure is not actually damaged and the whole process becomes reversible. Furthermore, by addressing the problem of damage location in a restricted situation of damage is at place A or place B or place C etc.., the problem becomes one of classification and can be dealt with by using pattern recognition algorithms.

2.1. Test structure

The wing had in total five inspection panels which could be used for the test (Figure 1). Two of the panels were used for the first two-class damage location problem and the other three for the subsequent three-class problem. The choice of the separate group of panels between the two-class and the three-class problems was mainly made due to the convenience that their location was offering (i.e. each group was clustered together).

Each panel was fixed to the wing by eight screws. Inevitably, their sequential removal introduced a certain degree of variability to the problem (change of the boundary conditions on the panel), as previous experience had already shown [20]. To alleviate this problem, the screws were secured and removed in the same order throughout the test with the help of an electric screwdriver with a controllable torque while using the same torque setting all the time.

2.2. Data acquisition for the two-location problem

The acquisition system used during the test was a DIFA Scadas III controlled by LMS software running on a DELL desktop PC. The sensors used were piezoelectric accelerometers of the PCB type. The base measurements were transmissibility functions across each panel, as they had previously proved effective [20, 21]. In addition, transmissibility functions do not need the accurate measurement of the excitation force. In a similar way to the previous work [20, 21], only the transmissibilities measured directly across each panel were used in this study. They were named as T1 and T2, where 'T1' means the transmissibility function 'across' Panel 1 and 'T2' the one 'across' Panel 2. A transmissibility function can be formed by taking the ratio of two FRFs. In the work here, the transmissibilities were formed by using a central accelerometer as a reference as seen in Figure 1. In addition, the same excitation levels were used during all testing (healthy state, added mass, saw-cuts) in order for the approach to be consistent. Further references on the concept of transmissibility can be found in [22].

All measurements were obtained within a frequency bandwidth of 0-2000 Hz at a resolution of 0.625 Hz. Previous work in [20], had shown that in order to acquire 'damage' sensitive

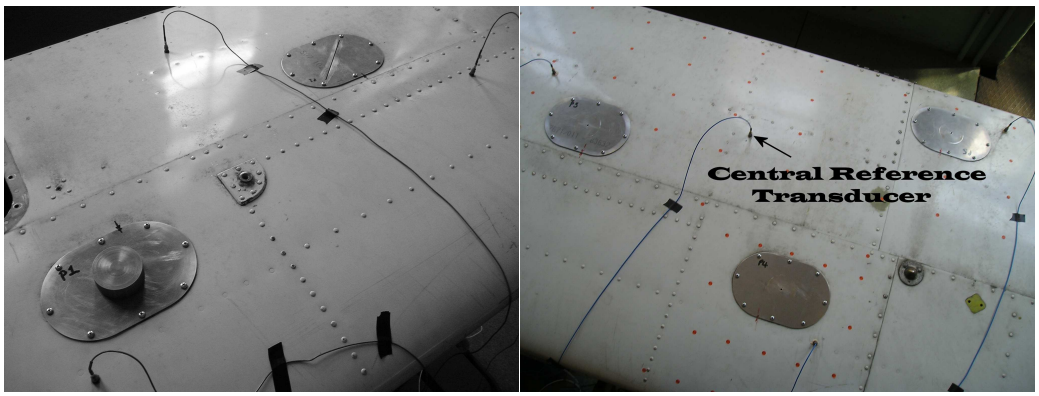

Figure 1: An example of an added mass and of a panel with a saw-cut are shown along with the location of the two panels which were used for the two-class problem (left), and an illustration of the three panels and reference transducer used in the three-class study (right).

features when inspection panels were fully removed, a frequency range of 1024 to 2048 Hz was needed. However, because of the added mass used here, the frequency bandwidth was chosen to be 0-2000 Hz so there would be a broader option for the selection of features. At this stage only the logarithm of the magnitudes of the data were used, the phase was discarded.

The wing was excited using a Gearing & Watson (G & W) electrodynamic shaker attached directly to its lower surface. A white Gaussian excitation was generated within the acquisition system and amplified using a G & W power amplifier. The excitation itself was measured using a standard PCB force transducer, but it was not directly used for the calculation of the transmissibilities.

The whole test order and configurations can be seen in the following:

1. Normal condition (all plates in place on the wing and intact).
2. Mass added (500 g) on Plate 1 on the wing.
3. Mass added (500 g) on Plate 2 on the wing.
4. Normal condition.
5. Faulty Plate 1 (diagonal saw-cut) replaces normal panel on the wing.
6. Faulty Plate 2 (diagonal saw-cut) replaces normal panel on the wing.
7. Normal condition.
8. Mass added (500 g) on Plate 1 on the wing.
9. Mass added (500 g) on Plate 2 on the wing.
10. Normal condition.
11. Faulty Plate 1 (diagonal saw-cut) replaces normal panel on the wing.
12. Faulty Plate 2 (diagonal saw-cut) replaces normal panel on the wing.
13. Normal condition.

Overall this meant that five sets of measurements for normal condition were taken and two sets for each damage scenario, first the added masses and subsequently the saw-cuts. For each of the 13 configurations a clean signal with 100 averages was acquired (in the estimation of the FRFs), to be used as a reference in the feature selection stage later and then 100 sequential measurements with only two averages.

In total, this gave 500 2-average measurements for the normal condition and 200 for each of the faulty states. The main reason for the second repetition of the test was simply to check and monitor the variability caused due to the removal and reattachment of the plates, making it thus an inherent part of the whole detection methodology. The same reasoning determined the number of normal sets so that there would be one healthy set after each fault.

2.3. Data acquisition for the three-location problem

For the three-location problem the acquisition system used was identical to that in the two-class problem, a DIFA Scadas III controlled by LMS software running on a DELL desktop PC. All measurements were obtained within the same frequency bandwidth described in §2.2 with accelerometers again used in order to create transmissibility functions. In a similar way the transmissibilities which were used were those measured directly across the inspection panels and were named as 'T3', 'T4' and 'T5' corresponding to panels 3,4 and 5 respectively (see again Figure 1). The test order maintained a similar configuration as before with normal conditions sets followed by added masses (on three panels this time), then normal conditions again followed by plates with saw-cuts. Overall this gave again five sets of normal condition and two repetitions for each of the 'faulty' states. In the three-class problem 40 averages were used for the clean signals (to be used for feature selection). In a similar way as before 500 2-average measurements for the normal states were acquired and 200 for each faulty state.

3. Feature selection

Feature selection is arguably one of the most important stages in a structural health monitoring project. Here, it is treated in a similar way as in [18, 20] and aimed only at the selection of features for the detection of the added mass on the plates. Consequently, a feature is a region of the given transmissibility which separates unambiguously the normal condition data from the added mass data.

The process of selecting features described here involves an extensive visual scanning of the measured data (the transmissibility functions) in search of regions which separate the normal condition data from the damage data. To simplify this procedure, reducing the size of the database and abiding by the previous studies [20], the search was limited to one transmissibility only for each of the panels. This means that features for the added mass on panel 1 were considered only from T1 and in the same way T2 served only for the detection of the mass on panel 2. Because of the large number of available features, in previous work [20], potential features were judged as strong, fair or weak mainly because of the need for a certain objectivity (although the process remains stills subjective) in their selection. The criteria used for the characterisation of the features can be found in either of [18, 20] and are not going to be repeated here. Although the same guidelines were followed here as well, the final selection of features was made on the logarithmic magnitude values of the measurements and it was based on the ranking of their performance as novelty detectors.

This ranking was possible with the help of outlier analysis. This algorithm was described and validated in [20, 23]. Basically, a statistical model of the healthy system is created, based on normal data, and then subsequent data are tested to see if they are statistically consistent or inconsistent with the normal data. For this purpose a statistical test is used to compute a quantity called the Mahalanobis squared-distance (MSD) which is then compared to a threshold. The threshold depends on the dimension of the problem and it can be exclusive or inclusive whether

Table 1: List of the features which were finally selected for the detection of the added masses in the two-class problem.

	Feature	Transmissibility	Spectral lines
Added mass	1	T1	898-925
on panel 1	2	T1	2215-2245
Added mass	3	T2	781-834
on panel 2	4	T2	1095-1123

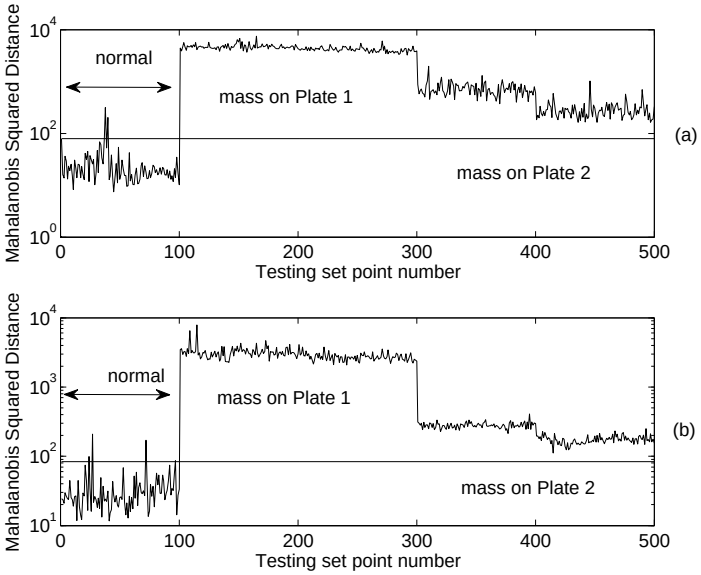

Figure 2: Outlier statistics for the two features selected from T1 to detect the added mass on panel 1.

the sample being tested is included or not in the computation of the Mahalanobis distance. The calculation of the threshold involves a Monte Carlo approach and is based on extreme value theory [24]. A comprehensive method of calculating the threshold is described in [23]. The ranking of the features was simply based on the Mahalanobis squared-distance normalised by the threshold. The Mahalanobis squared-distance is given by,

$$D_\zeta = (\mathbf{x}_\zeta - \overline{\mathbf{x}})^{\mathbf{T}}\mathbf{S}^{-\mathbf{1}}(\mathbf{x}_\zeta - \overline{\mathbf{x}}) \tag{1}$$

where $\mathbf{x}_\zeta$ is the potential outlier, $\overline{\mathbf{x}}$ is the mean vector of the sample observations and $\mathbf{S}$ the sample covariance matrix.

The transmissibility lines which were used for the finally selected features are shown in Table 1. When the dimension of the feature was greater than 40, the data were sub-sampled in order to avoid numerical issues in the inversion of the covariance matrix in the calculation of the MSD values.

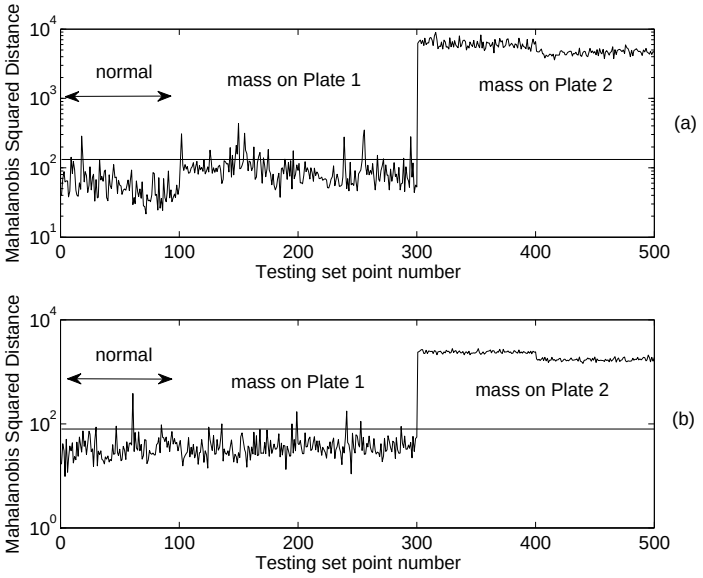

Figure 3: Outlier statistics for the two features selected from T2 to detect the added mass on panel 2.

4. Pseudo-fault location for the two-class problem

With the feature selection stage completed, there were four novelty detectors created by using outlier analysis on the selected features, two for each case of mass addition (Panel 1 or Panel 2). The novelty detectors were thus formed by the Mahalanobis squared-distance and can be seen in Figures 2 and 3. The use of more than one novelty detectors for each class was expected to make the approach more robust, as it would allow the Pattern Recognition algorithm to 'learn' more patterns. The constructed novelty detectors serve as identification of the presence of damage, so the damage detection problem is purely addressed as a restricted situation of the fault (mass or saw-cut here) being at one location (Panel 1 or Panel 2) at a time. By using this approach the problem reverts to one of classification.

In the current case, it was a simple dual-class problem and perhaps there are many classifiers which could perform well. However, the purpose of the work is to compare the scenario of added masses to that of saw-cuts (which represent realistic damage by the stiffness reduction they produce). Because of that, a consistent method had to be used and then be tested on 'damage' data. The one chosen here was the classification of the masses (Panel 1 or Panel 2) with the help of Artificial Neural Networks (ANN) since that was the approach already tried before in [20] with success. It is important to note that although the current problem has a dual-class nature similar to that of novelty detection, it is approached here in a supervised learning methodology.

In order to produce a level-two damage diagnostic (location problem) here, a standard Multi Layer Perceptron (MLP) network with one hidden layer was judged to be appropriate. The main idea was to map the novelty detectors created from the outlier statistics of the features which were selected from the transmissibilities, to the added mass location. The input layer of the network was presented with four novelty indices, since two of the best features were selected for

each added-mass location (Panel 1 or Panel 2).

The procedure for the training of the network followed the guidelines recommended by Tarassenko in [25]. All data were separated equally into training, validation and testing sets. The network structure had necessarily four input nodes, one for each of the novelty detectors and two output nodes, one for each class (mass location). The number of hidden nodes was a matter of investigation and had to be determined during training. In compliance with the accepted rule of thumb which suggests the existence of 10 patterns per weight [25] the search went from 1 hidden node up to 6. In addition 10 different random integer seeds for the weight initialisation were used. This means that, in total, 60 network structures were tested.

In order to estimate the classification accuracy of each network the *1 of M* strategy was employed. Each class is assigned a specific network output. Then, the network is asked to produce unity at the output which represents the input class and zero anywhere else during training. It can be shown, [26] that after training with this strategy, when the network is presented with an input, then the outputs of the network represent the Bayesian *a posteriori* probability that the input vector belongs to that class. The assigned class is simply the highest output, which represents the class with the highest probability. It should be noted that in this classification problem, it is assumed that there is only one fault at a time i.e. damage is at location A or at location B. Each of the assigned classes is assigned a prior probability, and in this case it is assumed that the probabilities are equal, meaning that all damage locations are equally likely before any data are observed. The number of training cycles used was originally tested with a maximum allowed limit of 100 and the optimisation algorithm for the network output error minimisation was the scaled conjugate gradients algorithm with the help of the NETLAB [27] package in MATLAB.

The validation set is used to discriminate between candidate network structures. Once the network structure has been selected and the network trained, its performance is evaluated using the testing set. The use of a different number of training cycles had an effect on the overall results, but because of the many networks giving excellent results on the mass-location problem it was not easy to decide what was the best choice. Therefore all of them were tried on the mass data and on the saw-cut data, as will be explained further on.

In Figure 4 there is a histogram of the classification rate of all the 60 networks tested after having been trained with a maximum of 100 cycles. It is clear that the dual-class problem of the added mass location is relatively simple for the classifier since all of the neural networks give excellent (100 %) results both in the validation and testing sets. In fact, although the number of training cycles was restricted to a maximum of 100, in most cases the optimisation algorithm converged faster and this is the main reason that a different number of training cycles was not investigated at this point. These results show the great degree of available choice regarding the structure of neural networks.

5. Performance of the pseudo-fault locator on 'real' damage data - two classes

The next task was to test the added mass locator on the 'real' damage case which was, as said before, a saw-cut on the inspection plates. Since there were actually many choices of different networks, all had to be tested for their performance. Figure 4 shows the histogram of the classification rate of the networks on damage data.

The results appeared to be very good and promising since there were 27 out of 60 networks giving excellent (100 %) classification rates. In addition more than half of the networks (44), perform with a classification rate higher than 90 %. The worst results were 50 % which is

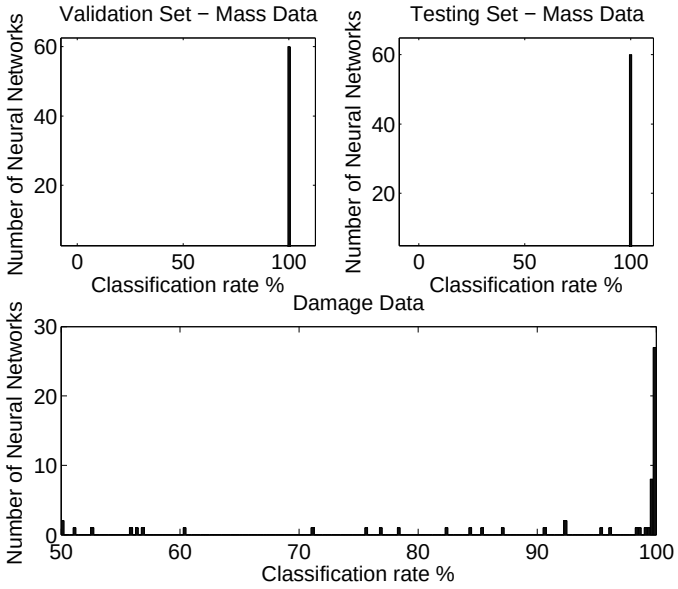

Figure 4: Histograms displaying the classification rate of all the neural networks which were tested for the two-class problem when they were trained with a maximum of 100 cycles.

equivalent to guessing for a dual-class problem, and were found only in two networks. The very encouraging results led to the decision to check how the novelty detectors that generated the features which were selected on the added mass data, would work on the damage (saw-cut) data.

In Figure 5 it can be seen that feature 1 performs very well on the damage data, in a similar way as in Figure 2 (mass data). The same cannot be said about feature 2 (in the same figure), since it appears to have a poor performance, although it still partially flags damage (only for one of the two repetitions). In Figure 6, both features (3 and 4) are shown to work very well on the saw-cut data, especially if they are compared with Figure 3. At this point, one may argue that the use of multiple novelty detectors for each class was crucial here, but further investigation had to be made before any solid conclusions were derived.

5.1. Principal component analysis for the two-class problem

In order to explain why there were networks which performed very well and few which performed very badly, Principal Component Analysis (PCA) was employed for the visualisation of the features in two dimensions. In Figures 7 - 14, all the four novelty detectors created for the two-class problem are analysed with the help of principal component analysis (PCA). The first four, Figures 7 - 10, show the four novelty detectors visualised (projected on the first two principal components) when all different 'states' (normal, added mass, saw-cut) were used in the PCA analysis at the same time. The application of PCA in such a way is able to show how the selected feature is able to separate the data into different 'states' (normal, added mass, saw-cut). In Figures 11 - 14 the saw-cut data are projected on the first two principal components of the added mass data. The reason for the two slightly different ways of the application of the method was that the second one (projection on the added mass data) represents more closely the problem

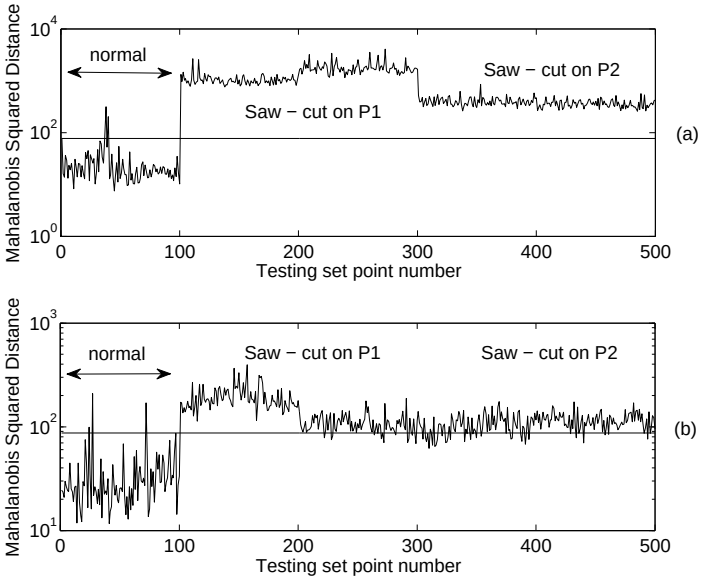

Figure 5: Performance (Outlier statistics) of the mass-selected features, for Panel 1 detection, on saw-cut data. Figure (a) corresponds to feature 1 and figure (b) to feature 2.

faced by the classifier, i.e. the neural network. At the stage of the creation of the novelty detectors the identification of the presence of damage has already been completed, so the neural network does not need the presence of normal data in order to classify the damage location.

The detailed inspection of all those figures confirms the results shown by the examination of the features' performance (see Figures 5 & 6) on the added mass and the saw-cut data. The existence of more than one cluster associated with the same class is caused by the repetitions of the experiment (5 for the normal state, 2 for each 'faulty' state), as described in the test procedure earlier. In the case where the complete feature vector (normal, mass, saw-cut data) was analysed through PCA, one can see a clear separation of the normal and the 'damaged' state (which the novelty detector was trained to locate), except for the second feature when compared on the saw-cut data (Figure 8), which was selected for the detection of the added-mass on Panel 1. Taking the previous statements into account, then it can be easily said that the objectives of the feature selection were indeed satisfied in three out of four features.

Discussing the above in more detail, the close comparison of Figure 8 with Figures 2 & 5 can reveal that data originating from the mass on Panel 1 are well separated with the normal data. The same cannot be said for data coming from the saw-cut on Panel 1 (data with the 'x' mark), since they overlap with some of the normal data in the PCA analysis and this confirms the outlier analysis results. Furthermore, there seems not to be a clear separation between the classes representing the saw-cut being on Panel 1 and on Panel 2, something which is very important in this classification problem.

The close examination of Figures 9 and 10 shows that both features succeed in separating the Panel 2 mass (and saw-cut as well) - data from the other states (normal, Panel 1 location). For this reason these two features seem to be 'ideal' for the localisation problem addressed here,

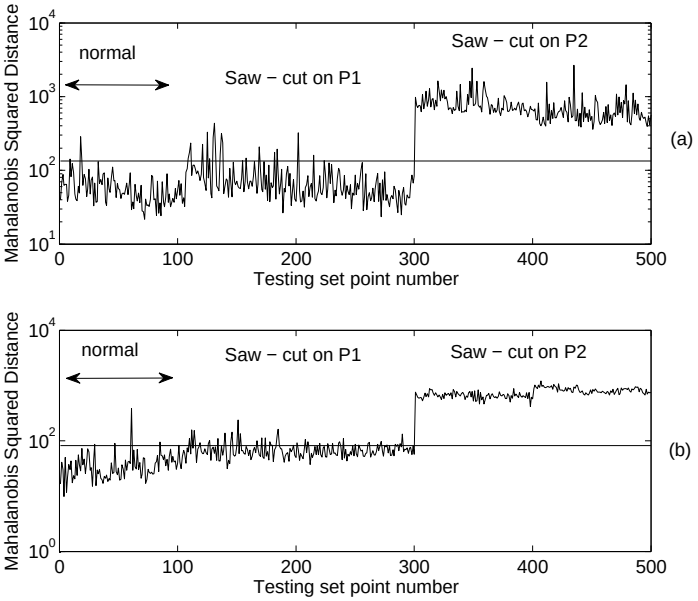

Figure 6: Performance (Outlier statistics) of the mass-selected features, for Panel 2 detection, on saw-cut data. Figure (a) corresponds to feature 3 and figure (b) to feature 4.

something already seen in the outlier analysis results as well. These PCA figures also reveal that there are many ways of separating the two classes (Panel 1 or Panel 2) well, both for the added mass and the saw-cut case. This is something which appears to be a good explanation of the classification results which showed some networks (27 out of 60) performing excellently (100 %) and 2 out of 60 very badly (50 %).

The examination of the PCA analysis on the feature data which were projected on the added mass data (Figures 11 - 14) strengthens this argument. A very good example of that is the potential decision boundaries drawn in Figure 11. If a classifier has been trained to separate between the mass on Panel 1 from the mass on Panel 2 by using the BB' line, then it would perform with an excellent classification rate in the saw-cut data as well. However, if the classifier was trained to separate between the two mass locations with the AA' line, then it would perform very badly on the saw-cut data.

Having said that here, one can also see (from the PCA figures) that there are indeed ways of separating equally well the mass and the saw-cut classes. In addition, a maximum margin classifier algorithm (e.g. support vector machines) would probably classify well both the added mass and the saw-cut data in the case presented in Figure 11, but it would not work well for the case presented in Figure 12. This was of course already proven from the fact that there were many networks (44 out of 60), which after having been trained on added mass data, performed very well (greater than 90% classification rate) on the saw-cut data. It is probably obvious from this discussion and the previous PCA results, that if there are overlaying mass and saw-cut features, then the classification rate will always be perfect and the problem of extracting 'damage-like' features without damaging the structure can be affordably solved. It was shown that the classes

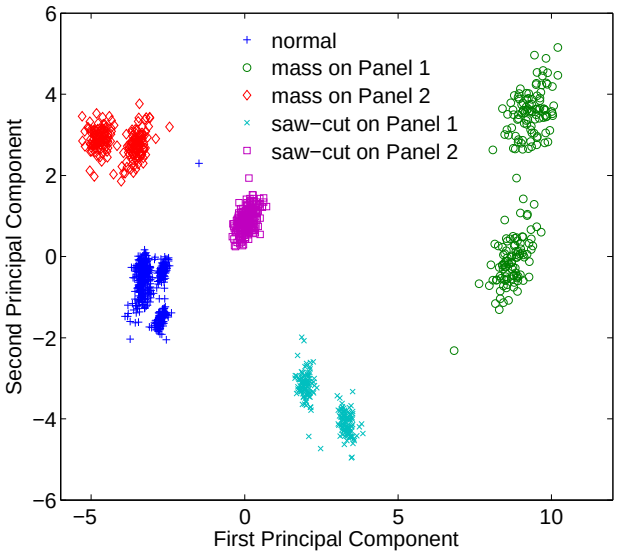

Figure 7: PCA visualisation of Feature 1, selected for the detection of mass on P1.

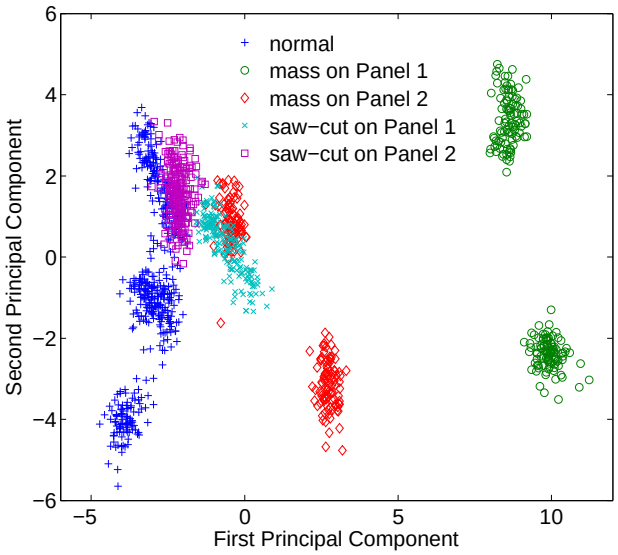

Figure 8: PCA visualisation of Feature 2, selected for the detection of mass on P1.

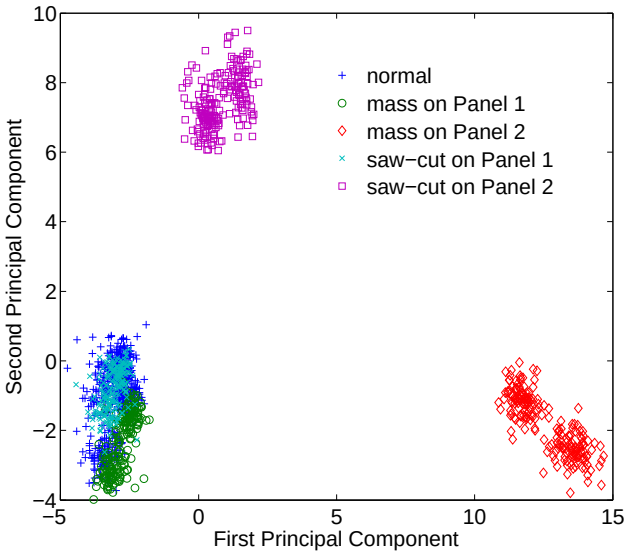

Figure 9: PCA visualisation of Feature 3, selected for the detection of mass on P2.

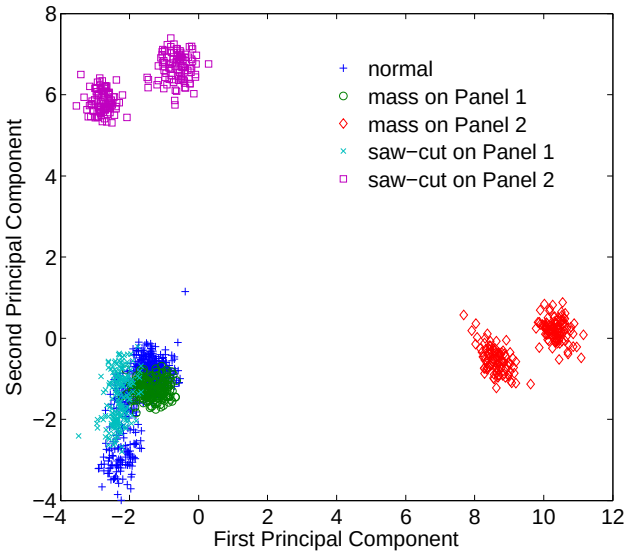

Figure 10: PCA visualisation of Feature 4, selected for the detection of mass on P2.

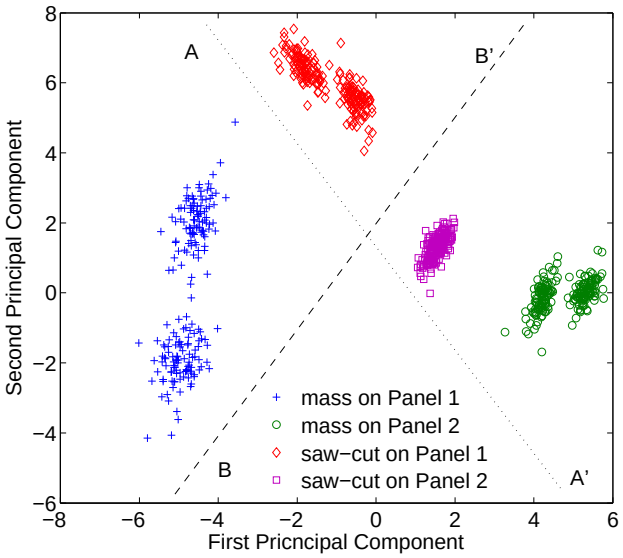

Figure 11: PCA visualisation of Feature 1, selected for the detection of mass on P1 with potential decision boundaries - data projected on the first two principal components of the added mass data.

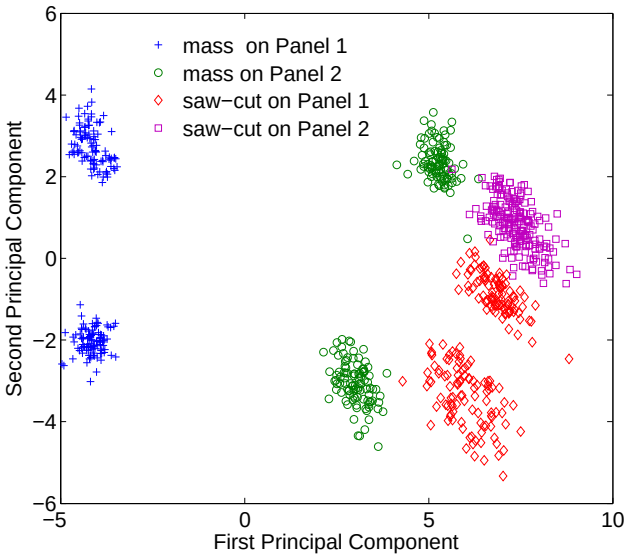

Figure 12: PCA visualisation of Feature 2, selected for the detection of mass on P1 - data projected on the first two principal components of the added mass data.

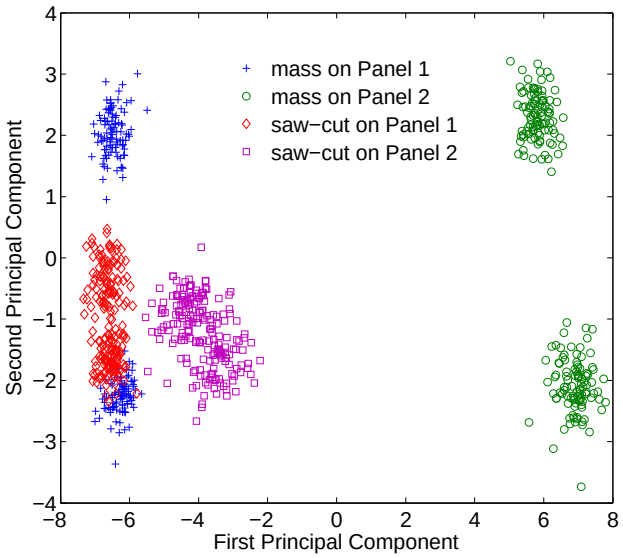

Figure 13: PCA visualisation of Feature 3, selected for the detection of mass on P2 - data projected on the first two principal components of the added mass data.

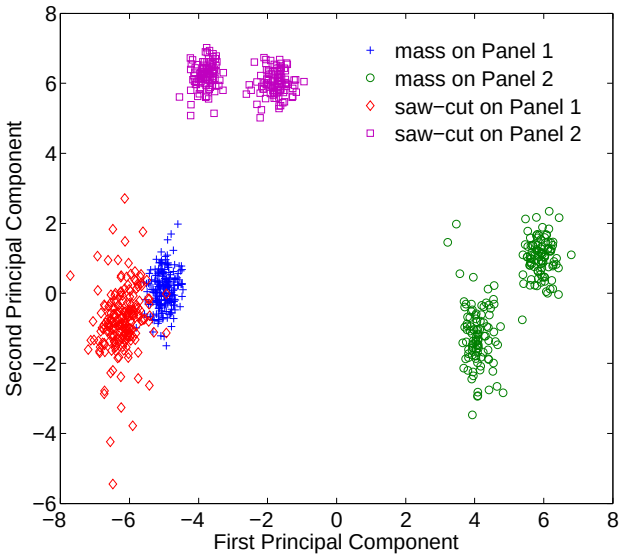

Figure 14: PCA visualisation of Feature 4, selected for the detection of mass on P2 - data projected on the first two principal components of the added mass data.

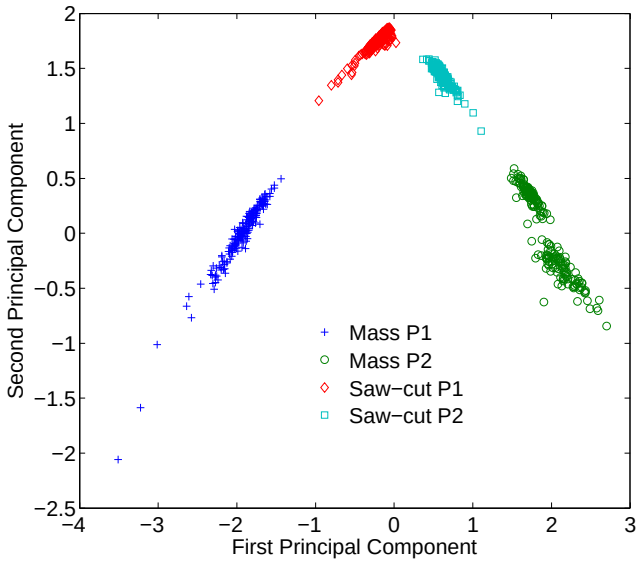

Figure 15: PCA visualisation of the four novelty detectors used as input to the neural network.

do not overlay in any situation and especially not when the saw-cut data were projected on the added mass data. In order to confirm this, the PCA algorithm was applied on the four novelty detectors which were used as inputs to the neural networks.

In Figure 15 the four novelty detectors are simply projected on the first two principal components of the added mass data. It is shown that all classes are easily separable and there are many ways to actually separate them. In fact the same example which was used in Figure 11 could be applied here as well and show why the training of the networks on the added mass data could fail in the classification of the saw-cut data. However, if the maximum linear classifiers are drawn in order to define the area containing the lines which separate perfectly the classes, the above statement will be more clearly demonstrated. To illustrate in an example what is meant by 'maximum linear classifiers', a simple schematic is shown in Figure 16. Two classes can be separated perfectly by one line, and in Figure 16, any line which can be found inside the shaded area defined by lines AA',BB',CC' and DD' separates perfectly the two classes shown.

The same example shown in the schematic of Figure 16 can be applied in the four novelty detectors used in the two-class problem. Figure 17 present the linear decision boundary areas which classify the added mass (a) and the saw-cut (b) data perfectly. The cross-area (the desirable area) which contains linear classifiers which would work for both the added mass and the saw-cut data is clearly shown in Figure 18 to be smaller than the added mass area. The probability therefore, of selecting linear classifiers based on the added masses which would then work on the saw-cut data is again small. The examination of the same figure also shows that the added mass area which is left outside the cross-area (non desirable area) is actually smaller than the desired cross-area, and this explains the high number of excellent networks (27 out of 60). It should be noted that the analysis discussed above and shown in Figures 17 and 18 was only done in a qualitative approach and is meant to serve as a demonstration of the argument that there are

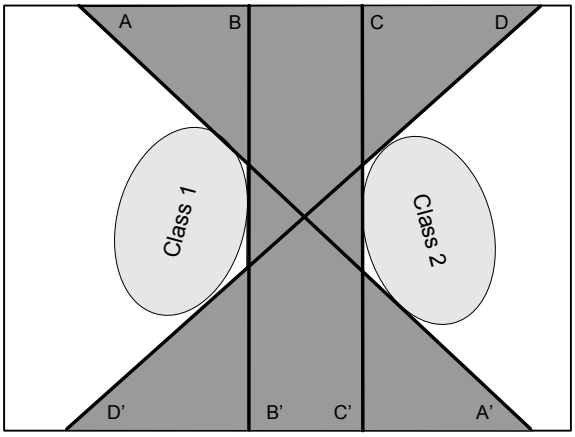

Figure 16: Schematic of potential linear decision boundaries for the classification of two classes.

ways to classify perfectly both the added mass and saw-cut data.

6. Three-class damage location

After the very promising classification results from the two-location problem the work was extended to a three-class localisation problem. The reason for this extension was explained in the introduction and it was mainly the fact that a three-class classification problem cannot be easily solved in an unsupervised learning approach. In addition, the extension of the approach in multiple locations (greater than two) can reveal the weaknesses of the overall methodology. The data acquisition procedure for the three-class challenge was similar to the two-class problem and was described in §2.2.

6.1. Feature selection for the three-class problem

The feature selection stage for the three-class problem was identical to the one followed for the two-class problem. Again, there was an extensive visual scanning of the transmissibilities in search of potential features which could form novelty detectors. The search was limited in one transmissibility for each of the panels (added mass locations), and the final selection was made on the logarithmic magnitude values of the measurements. The ultimate arbiter for the feature selection was again the same ranking scheme which was based on the Mahalanobis squared-distance.

The first preliminary attempt to build the added mass locator for the three panels consisted of the selection of two features for each panel (location) in exactly the same way as was done for the two-class problem. The transmissibility lines used for the six final features are listed in Table 2. From the outlier statistics of the six features, six novelty detectors were created in total. A standard MLP neural network was employed again, this time with six inputs and three outputs and was trained with the *1 of M* strategy. The novelty detectors created are not all shown here for the sake of space and avoiding the repetition of equivalent figures (with those from the two-class

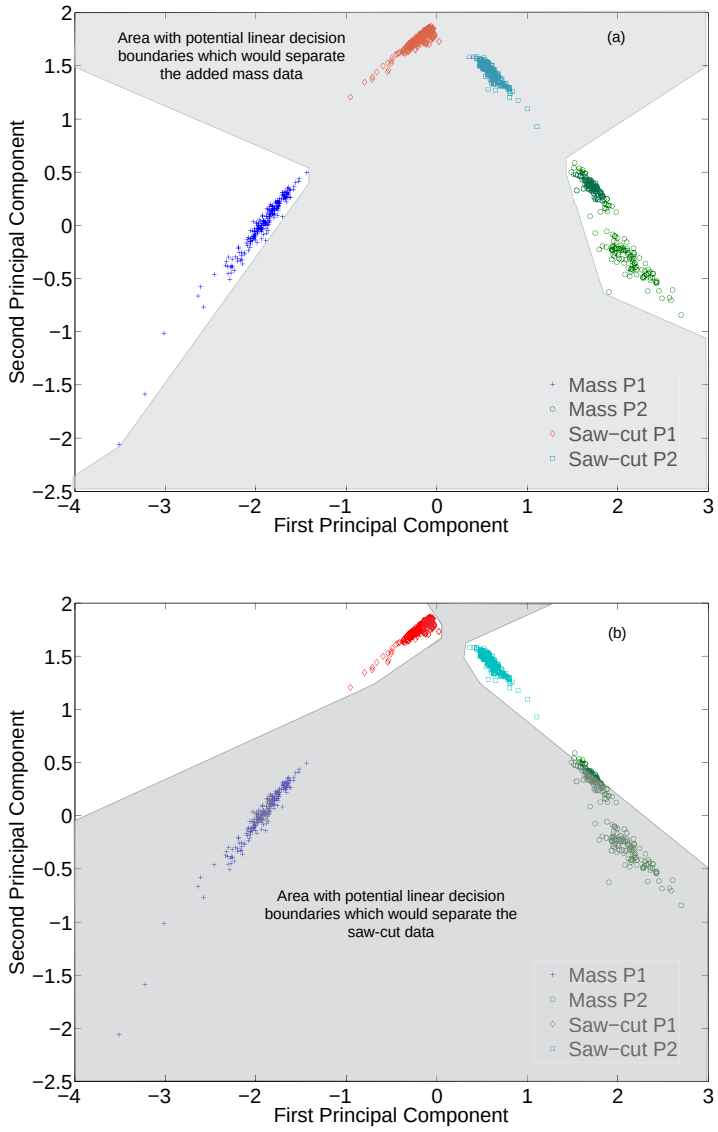

Figure 17: Areas defined by the maximum linear decision boundaries which separate the four novelty detectors from Figure 15. Figure (a) shows the linear boundaries which separate the added masse data and figure (b) the boundaries which separate the saw-cut data.

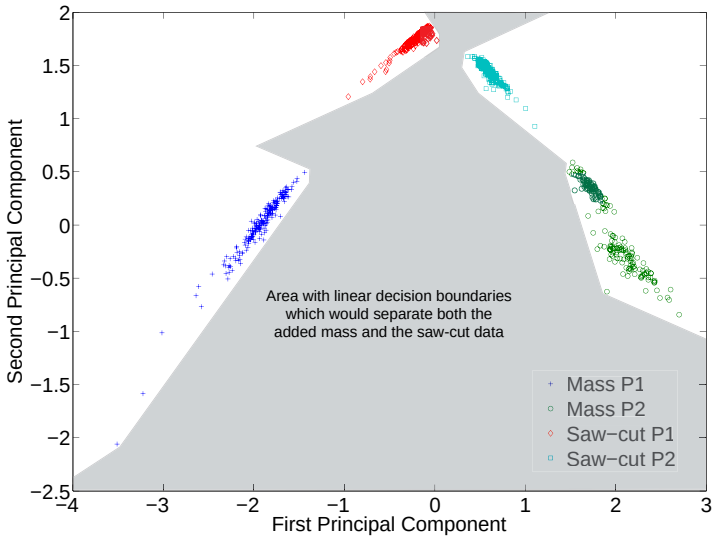

Figure 18: Cross-area (desired) defined by the linear decision boundaries which separate both the added mass and the saw-cut data.

problem). The results from this first attempt were significantly worse than the previous two-class problem. Although there were far too many choices (in terms of neural networks) for the added mass locator, when they were tested on the saw-cut data the majority of them performed with very low classification rates. Minimum performance was 33 %, which corresponds to guessing for a three-class problem.

6.2. Improving the performance of the three-class locator

The poor initial results of the three-class problem led to the decision to check the performance (outlier statistics) of the six selected features on the saw-cut data. It was clearly seen then that half of them did not indicate any presence of damage in the saw-cut data, or they displayed damage in the wrong panel, something which provides a possible explanation of the bad results. The PCA analysis of the two-class problem has clearly shown that ideally the features selected

Table 2: List of the features which were selected for the detection of the added masses in the three-class problem.

	Feature	Transmissibility	Spectral lines
Added mass	1	T3	140-162
on panel 1	2	T3	645-655
Added mass	3	T4	256-305
on panel 2	4	T4	860-910
Added mass	5	T5	250-265
on panel 3	6	T6	50-60

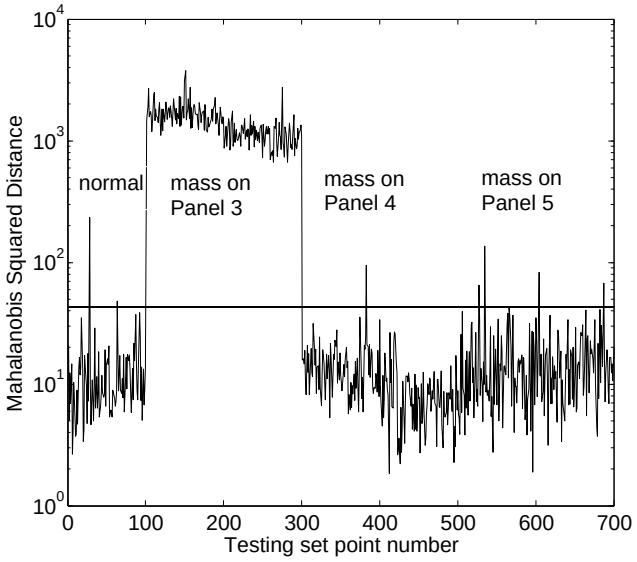

Figure 19: Outlier statistics for feature 3, selected from T3 for the detection of the added mass on Panel 1.

on the pseudo-faults (added mass here) should indicate the presence of the saw-cuts, as well as overlay when projected on their first two principal components. The possibility of actual features which work well in both cases (added mass - saw-cut) can be definitely considered crucial and attractive; however, before attempting to use the saw-cut data for the actual selection of features, it was considered more important to attempt to improve the damage location by further exploiting the added mass data only.

In the feature selection stage, the final selection criterion was the subjective ranking scheme described here in §3 and also in [18]. It was mainly based on the assumption that the best features for the added mass would be best for the saw-cuts (again see [18]) as well. The latter assumption led to the selection of features which were indicating damage in other panels as well as those they were intended to do. This extra 'damage' indication may have caused significant confusion to the neural network. Thus, it could be argued here that the network struggles to learn the difference among the classes in disarray (in the added mass data) and fails to learn the existing common patterns between the added mass and the saw-cut. In order to investigate the above claim it was decided to explore the performance of a locator trained only on novelty detectors indicating uniquely one panel. A thorough feature selection procedure was not considered necessary, since it had been already attempted in the relevant original feature selection stage here to find features with the previously described characteristics, but it was contradicting with the ranking scheme. As a compromise to the previous, the three (out of the original six) features which were most closely corresponding to the behaviour of indicating uniquely the added mass on the intended panel were used to create another damage locator. The performance of these features on added mass data can be seen in Figures 19-21, and on saw-cut data in Figures 22-24.

The new locator was based on a three input - three output MLP neural network. When it was tested on the saw-cut data it performed again with significantly lower classification rates than the

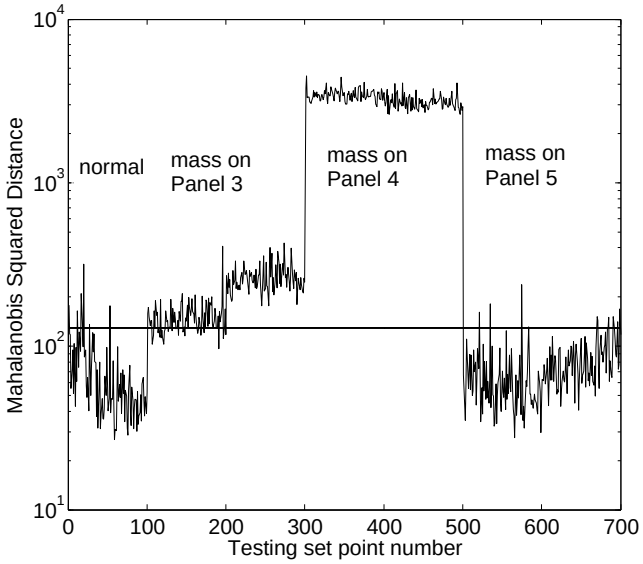

Figure 20: Outlier statistics for feature 4, selected from T4 for the detection of the added mass on Panel 2.

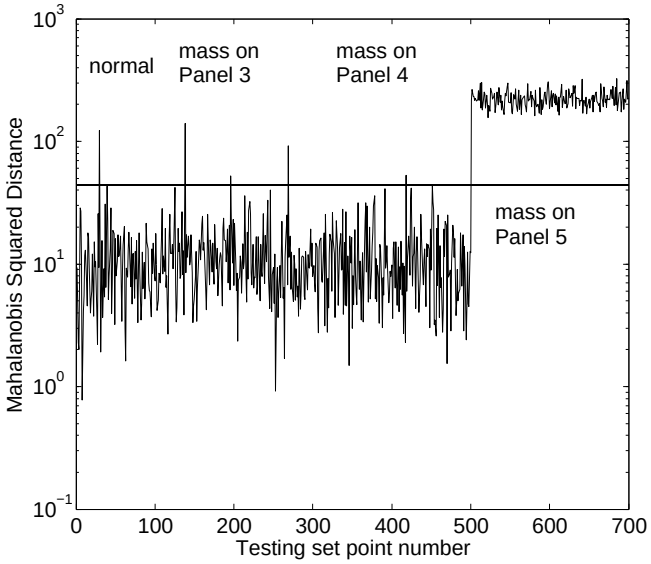

Figure 21: Outlier statistics for feature 5, selected from T5 for the detection of the added mass on Panel 3.

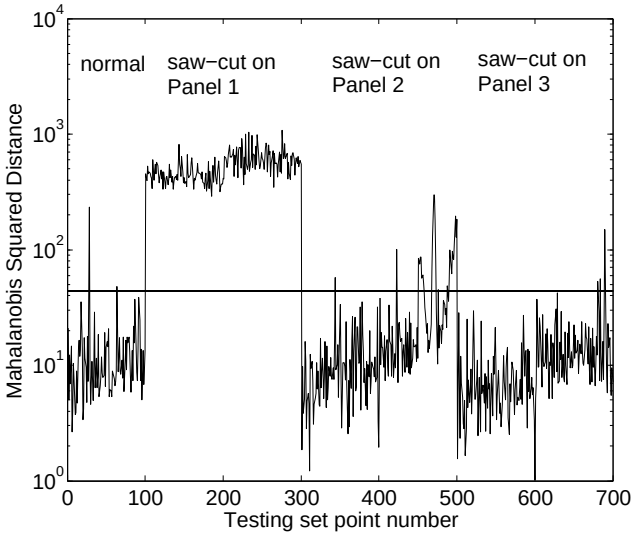

Figure 22: Outlier statistics for feature 3, selected to detect the mass on Panel 3, on saw-cut data.

two-class problem. Without commenting on the poor performance of feature 5 on saw-cut data (Figure 24), it should be noted that the idea that the neural networks get confused with multiple indication of mass in different panels had not been fully explored. Since it was observed that it was not trivial to find features which were ranked high, so they could probably work on the saw-cut data as well, and also to display single-panel only indication of 'damage', it was decided to modify the existing novelty detectors in order to create the desired characteristics. There were some important points to be taken into account regarding the modification of the novelty detectors. The process had to be done in a consistent way, and the parts of the novelty detectors which were indicating the desired panel location should by definition of the novelty detector not be altered. The latter was considered crucial so as not to conflict with the concept of the novelty detector, which is derived by some consistent process from features taken from the data. The main idea which was decided to be explored after the previous considerations was the setting of all the parts of the novelty detector which were below the threshold into zero. Recalling that the novelty detector is formed by the Mahalanobis squared-distance, the modification can be seen by,

$$\mathbf{D}_\zeta = \mathbf{D}_\zeta \, , \mathbf{D}_\zeta \geq D_T \tag{2}$$

$$\mathbf{D}_\zeta = 0 \quad , \mathbf{D}_\zeta < D_T \tag{3}$$

where $\mathbf{D}_\zeta$ is the Mahalanobis squared-distance and D_T is the threshold.

The examination of Figures 19-21 reveals that setting all the parts of the novelty detectors lower than the threshold to be zero, could produce the desired criteria for features 3 and 5, but not for 4. The latter required the additional raising of the threshold such that it would not display an added mass on panel 3 (see Figure 20 again). The raising of the threshold represents a principled tactic which can be used in a novelty detection approach and requires the use of damage data. Here, it is done only with the help of added mass data. The threshold was raised enough so

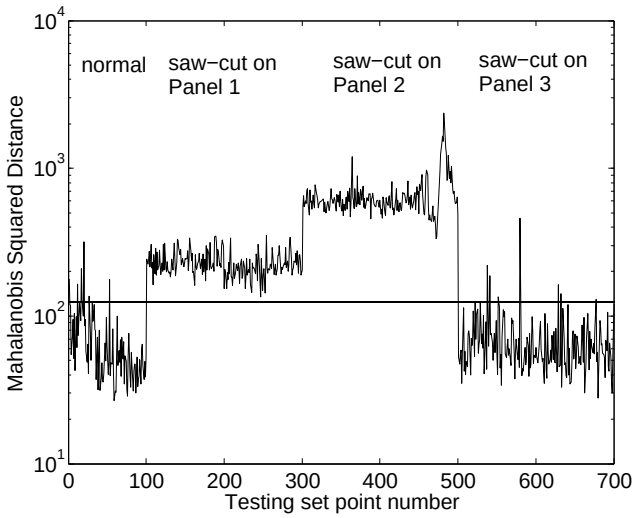

Figure 23: Outlier statistics for feature 4, selected to detect the mass on Panel 4, on saw-cut data.

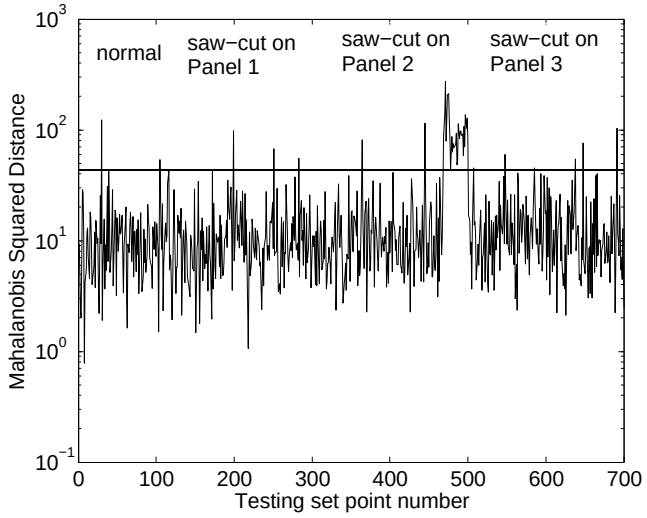

Figure 24: Outlier statistics for feature 5, selected to detect the mass on Panel 5, on saw-cut data.

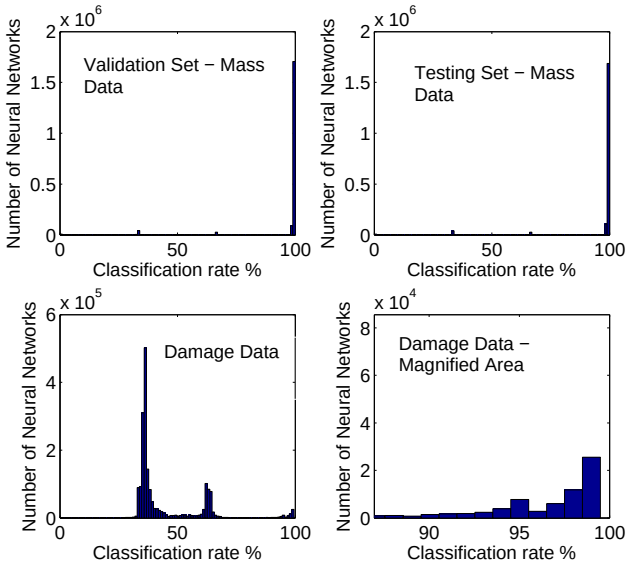

Figure 25: Histogram displaying the classification rate of all the neural networks (with different training cycles) tested with the modified novelty detectors for the three-class problem.

there would be no indication of damage (added mass) on panel 3. The new modified locator was tested again with similar settings as before. The maximum number of training cycles used was 200. Because of the many networks performing well on added mass data all of them were tested on saw-cut data as well. The results appeared to be slightly better than before since there were three networks performing with a higher classification rate of 90 %, with the best at 98 %, but only for 3 out of the total 80 networks tried. However, because of the few, but excellent results, it was decided to perform a more comprehensive investigation of the possible network structure which was used with the modified novelty detectors. It was previously mentioned that several networks were converging with less training cycles than the maximum allowed, but this time it was decided to force the training at specific numbers of iterations.

This time the search for the neural network structure had to be more thorough. The training cycles tested varied from 4 to 20 in increments of 4, and then from 30 to 200 with steps of 10. In order to explore the possibility of pure chance having an important effect, an option of no training cycles was also included in the search. The search for hidden units was allowed to go from 1 up to 8 units. The most crucial part of this analysis was the random seed for the weight initialisation of the neural networks which included 10,000 different numbers for each structure. In total 1,920,000 networks were tried and the results can be considered very interesting. In Figure 25 a histogram of the performance of all the networks is displayed. It was not surprising to see that the majority of the networks display a classification rate of 33 %, but a careful look in a magnified area of the plot shows that there are many excellent performances. In detail, there were 71001 networks with a classification rate over 80 %, 64279 of them were above 90 % and finally 1723 exceeding the excellent 99 %.

Because the histograms of Figure 25 do not give any information about the structure and the number of the training cycles which gave the high classification rate, a waterfall diagram is

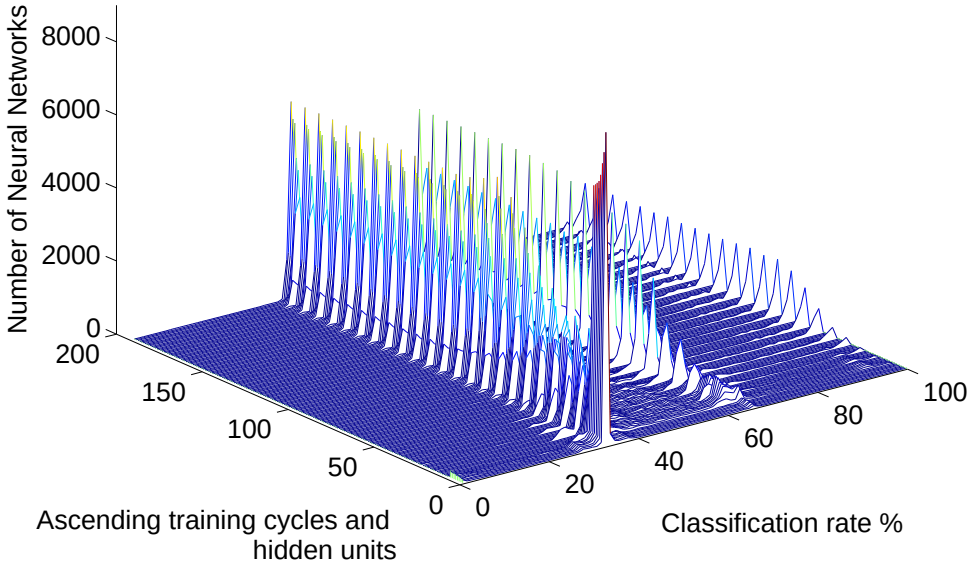

Figure 26: Waterfall diagram of the histograms displaying the classification rate of all the neural networks tested (three-class problem) against the number of training cycles (0 to 20, steps of 4, 20 to 200, steps of 10) and the number of hidden units (1 to 8).

presented in Figure 26. The histograms of the 10,000 networks generated with different random integer numbers (for the weight initialisation) for each structure and number of training cycles are plotted alongside in ascending order (regarding the training cycles and hidden units) in a waterfall representation. It is reminded here that for every number of training cycles there are eight different structures (1 - 8 hidden units) of neural networks. For example, in Figure 26 the x-axis displays the classification rate of the networks and the z-axis their number. The first value displayed in the y-axis corresponds to zero number of training cycles and a network structure of 1 hidden unit, and there are 10,000 networks randomly initialised with those settings. The following value in the same y-axis corresponds to zero number of training cycles again, but a network structure of 2 hidden units.

It can be clearly seen that there are some excellent performances in every network configuration after a number of training cycles (12), and the majority of them occur with one hidden unit. When the networks were left untrained, they performed almost entirely in the 33% classification region, something expected, since it is the statistical value for networks relying purely on chance in this problem.

The PCA analysis which was performed on the two-class problem would not provide any extra information on how the neural networks draw the decision boundaries, especially since the three classes would complicate the display of the maximum linear classifiers (at least two lines are needed to separate three classes). However, since the neural networks have three outputs it

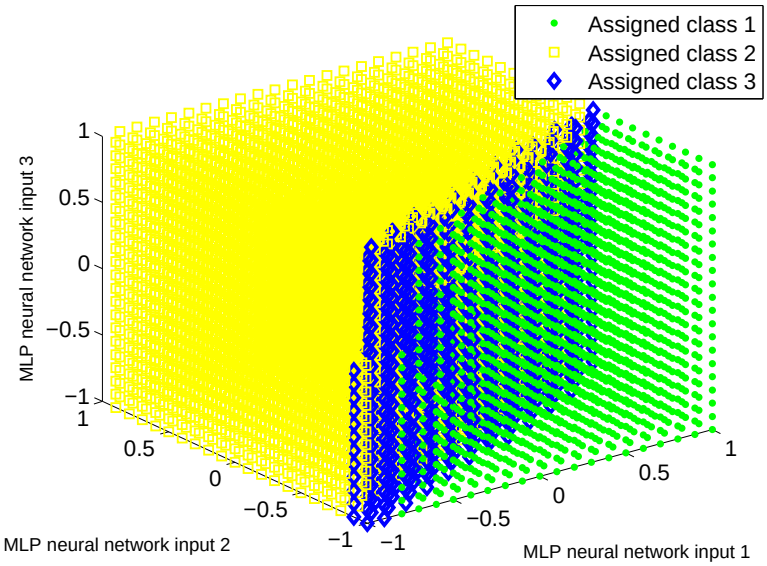

Figure 27: Visualisation of the assigned classes of an exemplar MLP neural network which had a correct classification rate of 99.5 % when presented with saw-cut data.

is feasible to visualise their decision boundaries on a three-dimensional plot. As the inputs to the networks are always normalised to be between -1 and 1, such a grid of numbers (between -1 and 1) can be passed through the neural network so that the highest output (the assigned class according to the *1 of M* strategy) can be coloured accordingly and provide an indication of the decision boundaries of the network. Figure 27 shows the visualisation of the decision boundaries of a trained MLP network (200 training cycles, 3 hidden units) which had a 99.5 % classification rate on the saw-cut data. It is interesting to see how the training data (added mass novelty detectors) and the damage data (saw-cuts) look like when plotted in three dimensions in Figures 28 and 29. It is clear in Figure 29 that there is more scatter on saw-cut data from the second location (second panel). The examination of the decision boundaries of networks with high classification rate and different structures and training cycles showed a similar pattern in the formation of the boundaries and show the sensitivity to the weight initialisation. Overall, this analysis confirms the PCA plots of the two-class problem and showed again that there are several ways to perfectly separate added mass and saw-cut data.

7. Discussion and Conclusions

This work aimed at the exploration of a non-destructive way of introducing damage to a structure by simply adding masses. The main goal was to use added masses to train neural networks and then test the constructed locator on 'real' damage data coming from saw-cuts. A Piper Tomahawk aircraft wing was the structure of interest here, and inspection panels on the wing were used in order to add masses and then introduce the saw-cuts. The problem was always addressed as one class at a time (i.e. one mass or one saw-cut) and involved two separate and subsequent studies of two and three classes. Novelty detectors capable of identifying the

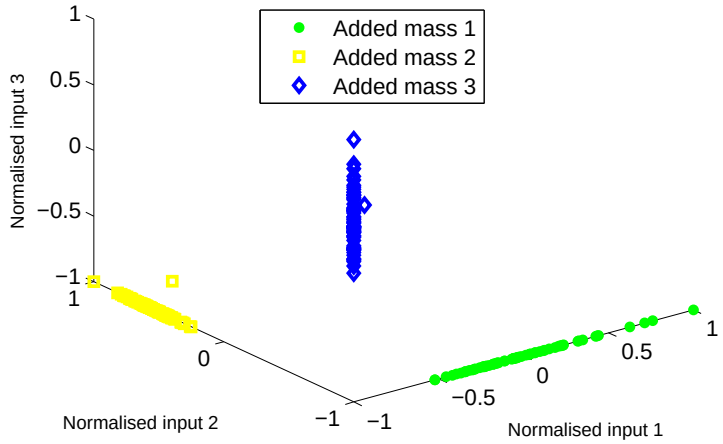

Figure 28: Normalised training set used (added mass novelty detectors) for the three-class problem plotted in three dimensions.

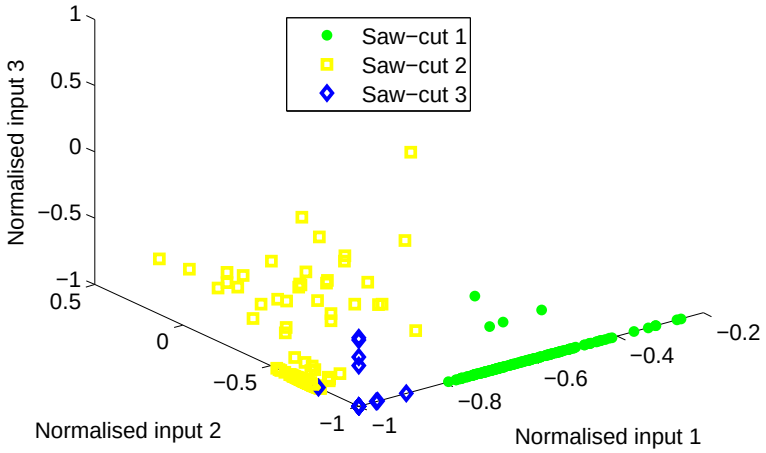

Figure 29: Normalised damage data (saw-cuts) for the three-class problem plotted in three dimensions.

presence of the added mass were created and then neural networks were used in order to classify the location of the mass with excellent success. The added mass locator was then tested on saw-cuts and performed very well for the two-class location problem, but poorly for the three-class problem.

An attempt to improve the results on the three-class problem employed the use of three novelty detectors, each of which indicated the presence of mass in one panel but not in any of the other panels. When it was not possible to find such novelty detectors, the existing ones were modified by the setting of their parts which were below the threshold into zero. In the case of the second feature, the raising of the threshold was necessary. The results were sufficiently interesting (and better than the first attempt) to initiate a comprehensive analysis of the effect of the neural network configuration (training cycles and structure) on the classification rate. It was found that there are excellent performances with various structures, but the majority of them appeared with one hidden unit, something which implies that there is no call for a complex network structure and correspondingly complex decision boundary. A subsequent visualisation of the selected features and novelty detectors via PCA showed that there are multiple ways of perfectly separating the classes for the two-class problem. A further visualisation of the neural network decision boundaries in the case of the three-class problem illustrated that although it is more challenging, there are again multiple ways of separating the classes.

The current work has showed that it is possible to use added masses in order to train neural networks and then identify the location of saw-cuts, since there were excellent locators for both the masses and the saw-cuts. However, in the work presented here, it was not possible to identify a complete experimental strategy for avoiding entirely the use of damage data , but this of course does not dismiss the possibility of such a strategy to be available with the use of different features or classifiers. Especially in the case of the two-class problem where there were many excellent locators (44 out of 60 networks tested having a greater than 90 % classification rate), an ensemble of neural networks [28] can be used to eliminate the networks which have a low success in the saw-cut data and fully avoid the use of damage data, and this can be presented in future work. In addition, the PCA analysis has shown that the ideal scenario would require an overlap of the added mass and saw-cut features, but this has proved to be very challenging. The latter fact in combination with the low complexity boundaries of the neural networks implies that the strategy of selecting very sensitive features to added mass may not be always appropriate for good generalisation in real structures. The authors believe that the use of pseudo-faults is one of the possible solutions to the problem of 'acquiring damage data without damaging the structure', and the use of added masses displays certain potential, especially if it is combined with other pseudo-faults or limited damage data.

Nevertheless, the authors also acknowledge the limitations of the approach. The extension of the problem to more classes as well as the effort to identify the location of multiple classes at the same time is probably going to be very challenging. In addition, even if a complete experimental strategy for the use of the added masses, without any use of damage data, is found, the extension of the approach to damage severity will be even more problematic. In any such case some sort of calibration scheme between added mass and stiffness reduction will probably have to be done. The lack of a universal way of introducing realistic damage into structures complicates any such severity attempt. The authors do not make any claim that added masses are equivalent to realistic damage, but as a localised 'disturbance' they can certainly be used to test a damage detection algorithm and as it was shown here, they can be used to train supervised learning algorithms. In the same spirit, different pseudo-faults could be of equivalent or even of higher value. An example of a different pseudo-fault is a localised heat increase as was considered in [29]. In

conclusion, supervised learning algorithms can indeed be trained with the use of surrogate data, and it is hoped that the current contribution will further help to stimulate the research on the subject of overcoming the frequent challenges met in PR approaches to SHM.

[1] J. E. Doherty, Handbook on Experimental Mechanics, Society for Experimental Mechanics, Inc., 1987, Ch. 12, Nondestructive Evaluation.

[2] S. W. Doebling, C. R. Farrar, M. B. Prime, D. Shevitz, Damage identification and health monitoring of structural and mechanical systems from changes in their vibration characteristics: A literature review, Tech. rep., Los Alamos National Laboratory LA-13070-MS (1996).

[3] H. Sohn, C. R. Farrar, F. M. Hemez, D. D. Shunk, D. W. Stinemates, B. R. Nadler, J. J. Czarnecki, A review of structural health monitoring literature: 1996-2001, Tech. rep., Los Alamos National Laboratory LA-13976-MS (2004).

[4] U. Baneen, N. Kinkaid, J. Guivant, I. Herszberg, Vibration based damage detection of a beam-type structure using noise suppression method, Journal of Sound and Vibration 331 (8) (2012) 1777–1788.

[5] E. Reynders, G. De Roeck, A local flexibility method for vibration-based damage localization and quantification, Journal of Sound and Vibration 329 (12) (2010) 2367–2383.

[6] H. Xu, L. Cheng, Z. Su, J.-L. Guyader, Identification of structural damage based on locally perturbed dynamic equilibrium with an application to beam component, Journal of Sound and Vibration 330 (24) (2011) 5963–5981.

[7] A. K. Pandey, M. Biswas, M. M. Samman, Damage detection from changes in curvature mode shapes, Journal Of Sound And Vibration 145 (2) (1991) 321–332.

[8] M. Friswell, Damage identification using inverse methods, Philosophical Transactions of the Royal Society A: Mathematical, Physical and Engineering Sciences 365 (1851) (2007) 393–410.

[9] J.-H. Park, J.-T. Kim, D.-S. Hong, D.-D. Ho, J.-H. Yi, Sequential damage detection approaches for beams using time-modal features and artificial neural networks, Journal of Sound and Vibration 323 (1-2) (2009) 451–474.

[10] U. Dackermann, J. Li, B. Samali, Identification of member connectivity and mass changes on a two-storey framed structure using frequency response functions and artificial neural networks, Journal of Sound and Vibration 332 (16) (2013) 3636–3653.

[11] C. R. Farrar, S. W. Doebling, D. A. Nix, Vibration-based structural damage identification, Philosophical Transactions Of The Royal Society Of London Series A-Mathematical Physical And Engineering Sciences 359 (1778) (2001) 131–149.

[12] J. Cattarius, D. Inman, Experimental verification of intelligent fault detection in rotor blades, International Journal of Systems Science 31 (11) (2000) 1375–1379.

[13] H. M. Kim, T. J. Bartkowicz, An experimental study for damage detection using a hexagonal truss, Computers & Structures 79 (2) (2001) 173–182.

[14] P. J. Fanning, E. P. Carden, Experimentally validated added mass identification algorithm based on frequency response functions, Journal Of Engineering Mechanics-Asce 130 (9) (2004) 1045–1051.

[15] W. Ostachowicz, M. Krawczuk, M. Cartmell, The location of a concentrated mass on rectangular plates from measurements of natural vibrations, Computers & Structures 80 (16-17) (2002) 1419–1428.

[16] J. S. Sakellariou, S. D. Fassois, Vibration based fault detection and identification in an aircraft skeleton structure via a stochastic functional model based method, Mechanical Systems And Signal Processing 22 (3) (2008) 557–573.

[17] K. Worden, L. Y. Cheung, J. A. Rongong, Damage detection in an aircraft component model, in: Proceedings of the 19th International Modal Analysis Conference, Vol. 4359, 2001, pp. 1234–1241.

[18] E. Papatheou, G. Manson, R. J. Barthorpe, K. Worden, The use of pseudo-faults for novelty detection in shm, Journal Of Sound And Vibration 329 (12) (2010) 2349–2366.

[19] A. Rytter, Vibration-based inspection of civil engineering structures, Ph.D. thesis, University of Aalborg, Department of Building Tecnhology and Structural Engineering (1993).

[20] G. Manson, K. Worden, D. Allman, Experimental validation of a structural health monitoring methodology: Part iii. damage location on an aircraft wing, Journal Of Sound And Vibration 259 (2) (2003) 365–385.

[21] G. Manson, K. Worden, D. Allman, Experimental validation of a structural health monitoring methodology: Part ii. novelty detection on a gnat aircraft, Journal Of Sound And Vibration 259 (2) (2003) 345–363.

[22] N. M. M. Maia, J. M. M. Silva, A. M. R. Ribeiro, The transmissibility concept in multi-degree-of-freedom systems, Mechanical Systems And Signal Processing 15 (1) (2001) 129–137.

[23] K. Worden, G. Manson, N. R. J. Fieller, Damage detection using outlier analysis, Journal Of Sound And Vibration 229 (3) (2000) 647–667.

[24] E. Castillo, Extreme value theory in engineering, Academic Press, Inc., 1988.

[25] L. Tarassenko, A Guide to Neural Computing Applications, Arnold, 1994.

[26] M. Bishop, Christopher, Neural Networks for Pattern Rcognition, Oxford University Press, 1995.

[27] I. T. Nabney, Algorithms for Pattern Recognition, Springer, 2001.

[28] M. P. Perrone, L. N. Cooper, Artificial Neural Networks for Speech and Vision, London : Chapman and Hall, 1993, Ch. When networks disagree: ensemble methods for hybrid neural networks, pp. 126–142.
[29] G. Manson, M. Matzakou, Shm feature selection using damage metaphors, in: Proceedings of the 25th International Conference on Noise and Vibration Engineering - ISMA2012, 2012, pp. 3345–3358.